

LONG-TERM TIMING AND GLITCH CHARACTERISTICS OF ANOMALOUS X-RAY PULSAR  
1RXS J170849.0-400910SINEM ŞAŞMAZ MUŞ<sup>1</sup>, ERSİN GÖĞÜŞ<sup>1</sup>  
*Draft version January 23, 2014*

## ABSTRACT

We present the results of our detailed timing studies of an anomalous X-ray pulsar, 1RXS J170849.0-400910, using *Rossi X-ray Timing Explorer* (*RXTE*) observations spanning over  $\sim 6$  yr from 2005 until the end of *RXTE* mission. We constructed the long-term spin characteristics of the source and investigated time and energy dependence of pulse profile and pulsed count rates. We find that pulse profile and pulsed count rates in the 2–10 keV band do not show any significant variations in  $\sim 6$  yr. 1RXS J170849.0-400910 has been the most frequently glitching anomalous X-ray pulsar: three spin-up glitches and three candidate glitches were observed prior to 2005. Our extensive search for glitches later in the timeline resulted in no unambiguous glitches though we identified two glitch candidates (with  $\Delta\nu/\nu \sim 10^{-6}$ ) in two data gaps: a strong candidate around MJD 55532 and another one around MJD 54819, which is slightly less robust. We discuss our results in the context of pulsar glitch models and expectancy of glitches within the vortex unpinning model.

*Subject headings:* pulsars: individual (AXP 1RXS J170849.0-400910) – stars: neutron – X-rays: stars

## 1. INTRODUCTION

Glitches, sudden jumps in the rotation frequency of neutron stars, are the unique events that provide invaluable information on the internal structure of extremely compact stars. Originally detected from rotation powered neutron stars (see e.g., Richards & Comella 1969; Radhakrishnan & Manchester 1969), glitches are generically not associated to changes in the radiative behavior of the source. (but see, Weltevrede et al. 2011). Therefore, the proposed glitch models involve dynamical variations in the neutron star interior instead of an external torque mechanism. The size of the glitch typically reflects the underlying internal dynamics of the neutron star: small-size glitches ( $\Delta\nu/\nu \sim 10^{-9}$ , aka. Crab-like glitches) are explained by the decrease of the moment of inertia of the pulsar (Ruderman 1969; Baym & Pines 1971) and large-size glitches ( $\Delta\nu/\nu \sim 10^{-6}$ , aka. Vela-like glitches) are described as the angular momentum transfer from inner crust neutron superfluid to the crust by the sudden unpinning of the vortices that are pinned to the inner crust nuclei (Anderson & Itoh 1975; Pines et al. 1980).

Anomalous X-ray Pulsars (AXPs) are slowly rotating ( $P \sim 2\text{--}12$  s) neutron stars with persistent emission being significantly in excess of their inferred rotational energy loss rate. So far, there has been no evidence of binary signature in AXPs. They are young systems ( $\sim 10^4$  yr) as inferred from their characteristic spin-down ages ( $P/2\dot{P}$ ), and also supported by their location on the plane of Milky Way, and the association of at least five AXPs with their supernova remnants. Almost all AXPs emitted short duration, energetic bursts in X-rays (see, e.g., Gavril et al. 2002; Kaspi et al. 2003 and for a recent review Rea & Esposito 2011). Their surface dipole magnetic field strengths inferred from their periods and

spin-down rates are on the order of  $10^{14} - 10^{15}$  G, which is much higher than that of conventional magnetic field strengths of pulsars. The decay of their extremely strong magnetic fields is proposed as the source of energy for their persistent X-ray emission and burst activity (Thompson & Duncan 1995, 1996; Thompson et al. 2002). Recently, observational evidence of dipole field decay was reported by Dall’Osso et al. (2012).

Glitch activity from an AXP was first seen in 1RXS J170849.0-400910 (Kaspi et al. 2000). Thanks to almost continuous spin monitoring of AXPs with *RXTE* for more than a decade, sudden spin frequency jumps have now been observed from six AXPs (see, e.g., Kaspi et al. 2003; Dall’Osso et al. 2003; Woods et al. 2004; Morii et al. 2005; Israel et al. 2007a,b; Dib et al. 2008, 2009; Gavril et al. 2011). Fractional glitch amplitudes ( $\Delta\nu/\nu$ ) of these events range from  $10^{-8}$  to  $10^{-5}$  (Dib et al. 2009; İċdem et al. 2012) and fractional post-glitch change in spin-down rates ( $\Delta\dot{\nu}/\dot{\nu}$ ) are between  $-0.1$  and  $1$  (Kaspi et al. 2003; Dib et al. 2009).

Glitches from AXPs somehow resemble those from radio pulsars, but contain some peculiar distinctive features in their recovery behavior and associated radiative characteristics (Woods et al. 2004; Morii et al. 2005; Dib et al. 2008, 2009; Gavril et al. 2011). AXP 1E 2259+586 went into an outburst in conjunction with a glitch (Kaspi et al. 2003; Woods et al. 2004). AXP 1E 1048.1-5937 has shown X-ray burst correlated with a glitch event (Dib et al. 2009). During the burst active phase of AXP 4U 0142+61 between 2006 and 2007, six short bursts and a glitch with a long recovery time were observed (Gavril et al. 2011). AXP 1E 1841-045 has exhibited bursts and glitches, but not coincidentally (Dib et al. 2008; Zhu & Kaspi 2010; Kumar & Safi-Harb 2010; Lin et al. 2011). Israel et al. (2007b) reported a burst and an extremely large glitch ( $\Delta\nu/\nu \sim 6 \times 10^{-5}$ ) from CXOU J164710.2-455216, but the possibility of such a glitch was ruled out by Woods et al. (2011). How-

sinemsm@sabanciuniv.edu

<sup>1</sup> Sabancı University, Faculty of Engineering and Natural Sciences, Orhanlı–Tuzla, 34956 Istanbul Turkey

ever, the latter team point out that a glitch with the size of usual AXP glitches may indeed have occurred. 1RXS J170849.0-400910 has been the most frequently glitching AXP (Kaspi et al. 2000, 2003; Dall’Osso et al. 2003; Israel et al. 2007a; Dib et al. 2008), but it has not shown any bursts or remarkable flux variability related to the glitch epochs.

It is still unclear whether glitches are always associated with radiative enhancements. Recently, Pons & Rea (2012) suggested that in the context of the starquake model, glitches observed in the bright sources can be related to the radiative enhancements but due to the bright quiescent state of these sources and fast decay of the enhancements, these events can be observed as small changes in the luminosity or only detected in faint sources.

1RXS J170849.0-400910 is an AXP with a spin period of  $\sim 11$  s. After the discovery of its spin period (Sugizaki et al. 1997), it has been monitored with *RXTE* for  $\sim 13.8$  yr. Analyzing the first  $\sim 1.4$  yr of data Israel et al. (1999) and Kaspi et al. (1999) have concluded that the source is a stable rotator. The continued monitoring has been essential in detecting three unambiguous glitches and three glitch candidates without any significant pulse profile variations (Kaspi et al. 2000, 2003; Dall’Osso et al. 2003; Israel et al. 2007a; Dib et al. 2008). There appears to be a correlation between intensity and spectral hardness: the X-ray spectrum gets softer (harder) while the X-ray flux decreases (increases), possibly in relation with glitches (Rea et al. 2005; Campana et al. 2007; Rea et al. 2007; Israel et al. 2007a). Götz et al. (2007) reported the same correlation in the hard X-rays using *INTEGRAL*/ISGRI data. However, den Hartog et al. (2008) claimed that they did not find the reported variability in their analysis. Thompson et al. (2002) proposed that external magnetic field can twist and untwist. Twisting and untwisting of the external magnetic field can lead to cracks and unpin the vortices for the glitches (Thompson & Duncan 1996; Dall’Osso et al. 2003). Such twist/untwist of the magnetic field with a period of  $\sim 5$ – $10$  yr has been suggested as an explanation for the observed correlations (Rea et al. 2005; Campana et al. 2007).

Here, we report on the analysis of long-term *RXTE* observations of 1RXS J170849.0-400910 spanning  $\sim 6$  yr. In §2 we describe *RXTE* observations that we used in our analysis. We present long-term timing characteristics of the source in §3.1. In §3.2 & §3.3 we constructed the pulse profiles, calculated pulsed count rates and examined their variability both in time and energy. We present the results of our extensive search for glitches in §3.4. Finally, in §4 we discuss our results in the context of glitch models and expectancy of glitches in the vortex unpinning model.

## 2. *RXTE* OBSERVATIONS

1RXS J170849.0-400910 has been almost regularly monitored with *RXTE* in 528 pointings since the beginning of 1998. Phase connected timing behavior of the source was investigated by Dib et al. (2008) using the *RXTE* data collected between 1998 January 12 and 2006 October 7, Dall’Osso et al. (2003) using data from 1998 January 13 to 2002 May 29, and Israel et al. (2007a) using from 2003 January 5 to 2006 June 3. Here we ana-

lyzed *RXTE* data collected in 280 pointings between 2005 September 25 and 2011 November 17 with the Proportional Counter Array (PCA). Note that the first 49 pointings in our sample were also used by Dib et al. (2008). We included them in order to maintain the continuity in the timing characteristics of 1RXS J170849.0-400910. Exposure times of individual *RXTE* observations ranged between 0.25 ks (in one observation) and 2.5 ks, with a mean exposure time of 1.9 ks (see Figure 1 for a distribution of exposure times). For our timing analysis, we used data collected with all operating Proportional Counter Units (PCUs) in GoodXenon mode that provides a fine time resolution of  $1 \mu\text{s}$ .

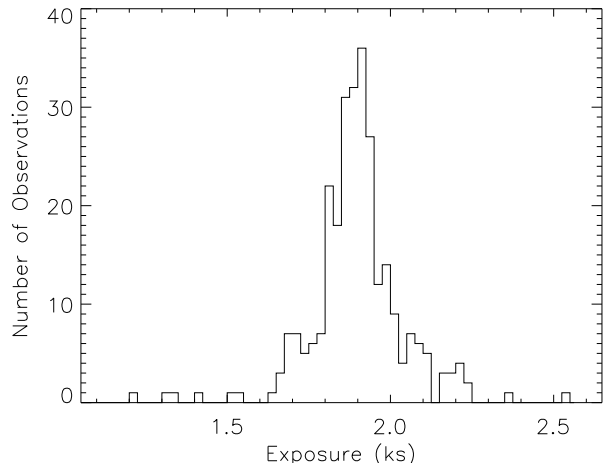


FIG. 1.— Distribution of exposure times of individual *RXTE*/PCA observations. The shortest observation with an exposure of 0.25 ks is excluded for clarity.

## 3. DATA ANALYSIS AND RESULTS

### 3.1. Phase Coherent Timing

We selected events in the 2–6 keV energy range from the top Xenon layer of each PCU in order to maximize the signal-to-noise ratio, as done also by Dib et al. (2008). All event arrival times were converted to the solar system barycenter and binned into light curves of 31.25 ms time resolution. We inspected each light curve for bursts and discarded the time intervals with the instrumental rate jumps. We merged observations together if the time gap between them was less than 0.1 days. The first set of observations (i.e., segment 0 in Table 1) which includes 49 observations from Dib et al. (2008) were folded initially with the spin ephemeris given by Dib et al. (2008) and later by maintaining the phase coherence. We then cross-correlated the folded pulse profiles with a high signal-to-noise template pulse profile generated from a subset of observations and determined the phase shifts of observations with respect to the template. We fitted phase shifts with

$$\phi(t) = \phi_0(t_0) + \nu_0(t - t_0) + \frac{1}{2}\dot{\nu}_0(t - t_0)^2 + \dots, \quad (1)$$

whose coefficients yield the spin frequency, and its higher order time derivatives, if required. In Table 1 we list the best fit spin frequency and frequency derivatives to the specified time intervals, obtained using also listed number of time of arrivals (TOAs). In Figure 2 (a) we present

the spin frequency evolution of 1RXS J170849.0-400910, and in (b) phase residuals after subtraction of the best fit phase model given in Table 1. We obtained frequency derivatives by fitting a second order polynomial to the sub-intervals of about 2.5 months long data and present them in Figure 2 (c).

### 3.2. Pulse Profile Evolution

We investigated long term pulse profile evolution of the source both in energy and time. For the pulse profile analysis, we excluded data collected with PCU0 and the data of PCU1 for the observations after 2006 December 25 due to the loss of their propane layers (therefore, having elevated background levels). We obtained the pulse profiles with 32 phase bins by folding the data in six energy bands with the appropriate phase connected spin ephemeris given in Table 1. The energy intervals investigated are 2–10 keV, 2–4 keV, 4–6 keV, 6–8 keV, 8–12 keV and 12–30 keV. In order to account for the different number of operating PCUs, we normalized the rates of each bin with the number of active PCUs. Finally, we subtracted the DC level and divided by the maximum rate of each profile. In Figures 3 and 4, we present the normalized pulse profiles for the six segments given in Table 1 in six energy bands and their evolution in time.

The 2–10 keV pulse profiles of 1RXS J170849.0-400910 are characterized by a broad structure formed by the superposition of two features: the main peak near the pulse phase,  $\phi \sim 0.55$  and a weaker shoulder around  $\phi \sim 0.85$ . Pulse profiles of the two lowest energy bands exhibit an additional shoulder (near phase  $\sim 0.35$ ) in the 55203 – 55516 epoch (Segment 4), which is not clearly seen in any other epochs. Pulse profiles in the 2–4 keV band consist of the main peak in all epochs, while the shoulder feature ( $\phi \sim 0.85$ ) is either weak or non-existent. The shoulder appears in the 4–6 keV band, and becomes more dominant above 6 keV. Pulse profiles above 8 keV contain only the shoulder feature. Note the fact that the duty cycle of the pulse profiles drops with increasing energy. The dominance of the secondary peak (shoulder) with the increase in photon energy was also reported in den Hartog et al. (2008) by using *INTEGRAL*, *XMM-Newton* and earlier *RXTE* observations.

We calculated the Fourier Powers (FPs) for a quantitative measure of the pulse profile variations. First we computed the Fourier transform of each profile and calculated the powers in the first six harmonics as  $FP_k = 2(a_k^2 + b_k^2)/(\sigma_{a_k}^2 + \sigma_{b_k}^2)$ . Here  $a_k$  and  $b_k$  are the coefficients in the Fourier series, and  $\sigma_{a_k}$  and  $\sigma_{b_k}$  are the uncertainties in the coefficients  $a_k$  and  $b_k$ , respectively. Second, we corrected the powers for the binning using equation 2.19 of van der Klis (1989) and calculated upper and lower limits to the FPs by using the method described in Groth (1975) (and also in Vaughan et al. 1994). Finally, we normalized the FPs by the total power. We show in Figure 5, the time evolution of the normalized harmonic powers in the first three Fourier harmonics. We find that the FPs remain fairly constant in time in all investigated energy intervals.

### 3.3. Pulsed Count Rates

PCA is not an imaging instrument; it collects all events originating within about  $1^\circ$  (FWHM) field centered near

the position of 1RXS J170849.0-400910. Therefore, we cannot construct a precise X-ray light curve of the source using PCA observations since the accurate determination of X-ray background with the PCA is not possible. Nevertheless, we can trace the behavior of the pulsed X-ray emission of 1RXS J170849.0-400910 since there is no other pulsed X-ray source with exactly the same pulse period in the vicinity. X-rays originating from the other sources in the field of view (even the pulsed ones) are averaged out after folding the data with the spin frequency of 1RXS J170849.0-400910 and remain within the DC level. For these reasons, we calculated the rms pulsed count rates of the source using

$$PCR_{\text{rms}} = \left( \frac{1}{N} \sum_{i=1}^N (R_i - R_{\text{ave}})^2 - \Delta R_i^2 \right)^{\frac{1}{2}} \quad (2)$$

$$\delta PCR_{\text{rms}} = \frac{1}{N PCR_{\text{rms}}} \left( \sum_{i=1}^N [(R_i - R_{\text{ave}}) \Delta R_i]^2 \right)^{\frac{1}{2}} \quad (3)$$

where  $R_i$  are the count rates in each phase bin,  $\Delta R_i$  are their uncertainties,  $R_{\text{ave}}$  is their average and  $N$  is the number of phase bins. Note that this is a background exempt representation of pulsed intensity of the source.

In Figure 2(d) we present the time variation of rms pulsed count rates in the 2–10 keV energy range. Here, each pulsed intensity value is an average of about 1 month of data accumulation. We find that the rms pulsed count rate in the 2–10 keV band does not show any significant variation. Figure 6 presents the pulsed count rates as a function of energy (in other words, rough energy spectra of the pulsed X-ray emission from 1RXS J170849.0-400910). Power law fits to these rough energy spectra yield a general trend from a more steep shape to a more shallow one as time progresses.

### 3.4. Search for Glitches

There is no explicit glitch detected in our data sample as it can be seen from the fit results to the phase drifts in Table 1. To investigate whether there are any small amplitude variations in phase drifts (i.e. frequency jumps), we fitted phase shifts using the MPFITFUN<sup>2</sup> (Markwardt 2009) procedure which performs Levenberg-Marquardt least-squares fit with the corresponding phases of a glitch model containing a jump in every  $\sim 0.1$  day and a linear decay, as follows:

$$\nu(t) = \nu_0(t) + \Delta\nu + \Delta\dot{\nu}(t - t_g) \quad (4)$$

where  $\nu_0(t)$  is the preglitch frequency evolution,  $\Delta\nu$  is the frequency jump,  $\Delta\dot{\nu}$  is the change of the frequency derivative after the glitch and  $t_g$  is the epoch of the glitch. First we applied this methodology to a previously published glitch in 2005 June and a candidate glitch in 2005 September. We detected the frequency jumps ( $\Delta\nu$ ) and glitch epochs in agreement with the published values (Israel et al. 2007a; Dib et al. 2008). We then carried out the glitch search in all six epochs listed in Table 1 as follows: For each epoch, we analyzed the fit results on the  $\Delta\nu$  versus the reduced  $\chi^2$  plane and identified the

<sup>2</sup> <http://purl.com/net/mpfit>

TABLE 1  
PULSE EPHEMERIS OF 1RXS J170849.0-400910 <sup>a</sup>

Parameter	Segment 0	Segment 1	Segment 2	Segment 3	Segment 4	Segment 5
Range (MJD)	53638 – 54056	54106 – 54421	54471 – 54786	54837 – 55151	55203 – 55517	55568 – 55882
Epoch (MJD)	53635.6772	54106.040	54471.050	54836.804	55202.849	55567.977
Number of TOAs	55	46	46	43	45	44
$\nu$ (Hz)	0.090884080(5)	0.090877558(5)	0.090872536(5)	0.090867590(3)	0.090862448(1)	0.090857386(7)
$\dot{\nu}$ ( $10^{-13}$ Hz s <sup>-1</sup> )	-1.55(2)	-1.50(1)	-1.43(2)	-1.642(5)	-1.641(1)	-1.73(2)
$\ddot{\nu}$ ( $10^{-22}$ Hz s <sup>-2</sup> )	-18(4)	-14(2)	-23(3)	1.9(4)	—	19(3)
$d^3\nu/dt^3$ ( $10^{-28}$ Hz s <sup>-3</sup> )	2.9(5)	0.9(2)	1.3(2)	—	—	-1.41(3)
$d^4\nu/dt^4$ ( $10^{-35}$ Hz s <sup>-4</sup> )	-1.7(2)	—	—	—	—	—
rms (phase)	0.0174	0.0145	0.0200	0.0212	0.0265	0.0203

<sup>a</sup> Values in parenthesis are the uncertainties in the last digits of their associated measurements

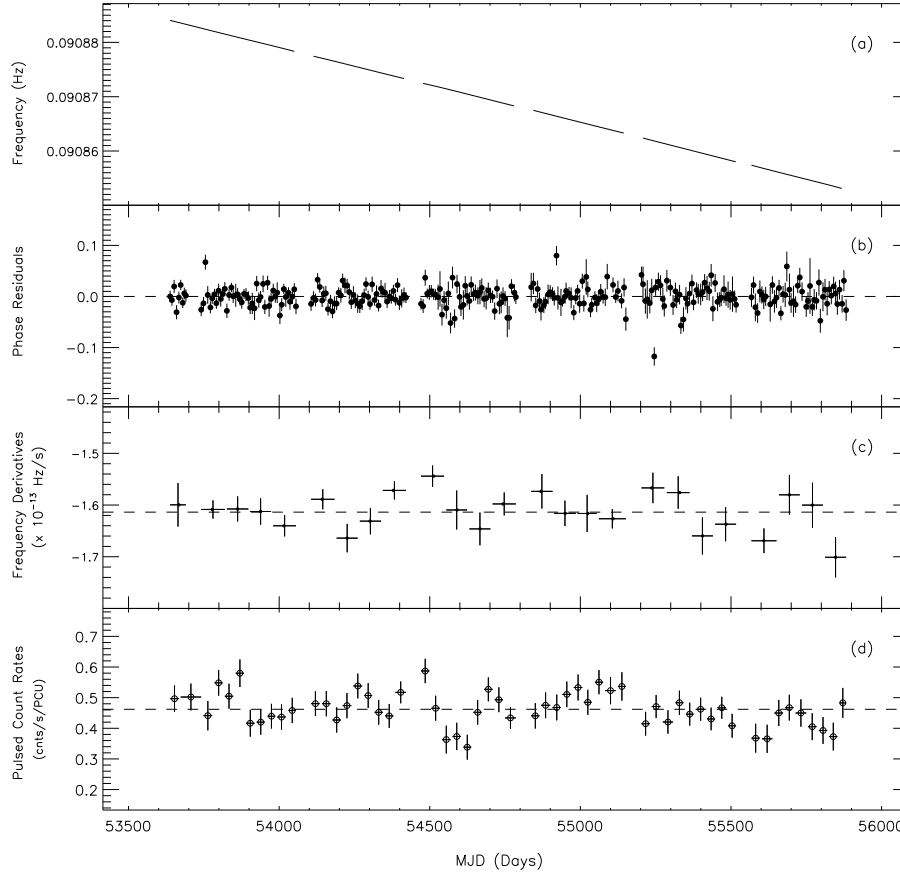


FIG. 2.— (a) Spin frequency evolution of 1RXS J170849.0-400910. (b) Phase residuals after the subtraction of the pulse ephemeris given in Table 1. (c) Frequency derivatives obtained using  $\sim 2.5$  months long data segments. (d) Long term behavior of the rms pulsed count rates in the 2–10 keV band.

set of parameters corresponding to the lowest reduced  $\chi^2$  value. We then computed rms fluctuations of phase residuals using the possible glitch parameters and compared them with those obtained using the polynomial fit results listed in Table 1. We find that rms phase residual fluctuations with respect to the glitch model fits do not indicate any improvement in the fit quality compared to the polynomial fits (Figure 7). Moreover, the largest glitch amplitude ( $\Delta\nu$ ) obtained is about  $3 \times 10^{-8}$  Hz in segments 0, 1 and 5 which could well be due to random fluctuations of phases, as can be seen in Figure 7.

Consecutive *RXTE* observations were typically performed at 7–10 day time intervals. Due to Sun con-

straints, there were five longer gaps of  $\sim 50$  days in our data set. In order to assess the probability for the detection of a glitch that might have occurred during these longer gaps, we adopted the detectability criterion defined as (Alpar & Ho 1983; Alpar & Baykal 1994):

$$\delta\nu + \delta\dot{\nu} * \Delta t \ll \Delta\nu \quad (5)$$

where  $\delta\nu$  and  $\delta\dot{\nu}$  specify the total error on the spin frequency and frequency derivative determined on both ends of the gap,  $\Delta t$  denotes the duration of the gap, and  $\Delta\nu$  is the change in spin frequency due to a putative glitch. Equation 5 implies that  $\Delta\nu$  has to be much bigger than maximum phase error accumulated across the

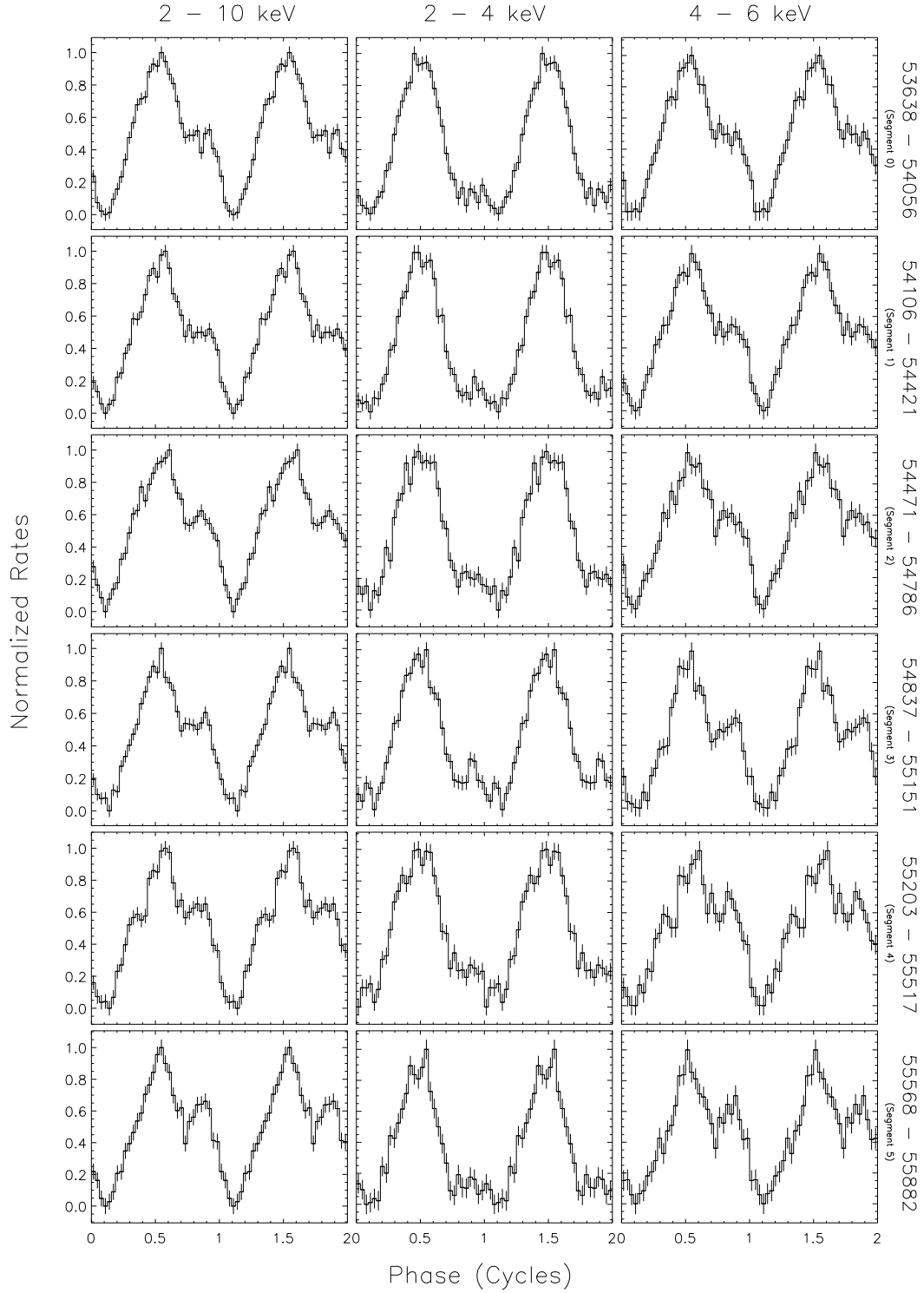


FIG. 3.— Pulse profile history of 1RXS J170849.0-400910 in the energy bands 2–10, 2–4 and 4–6 keV. The labels on the right are the corresponding time intervals of accumulated data.

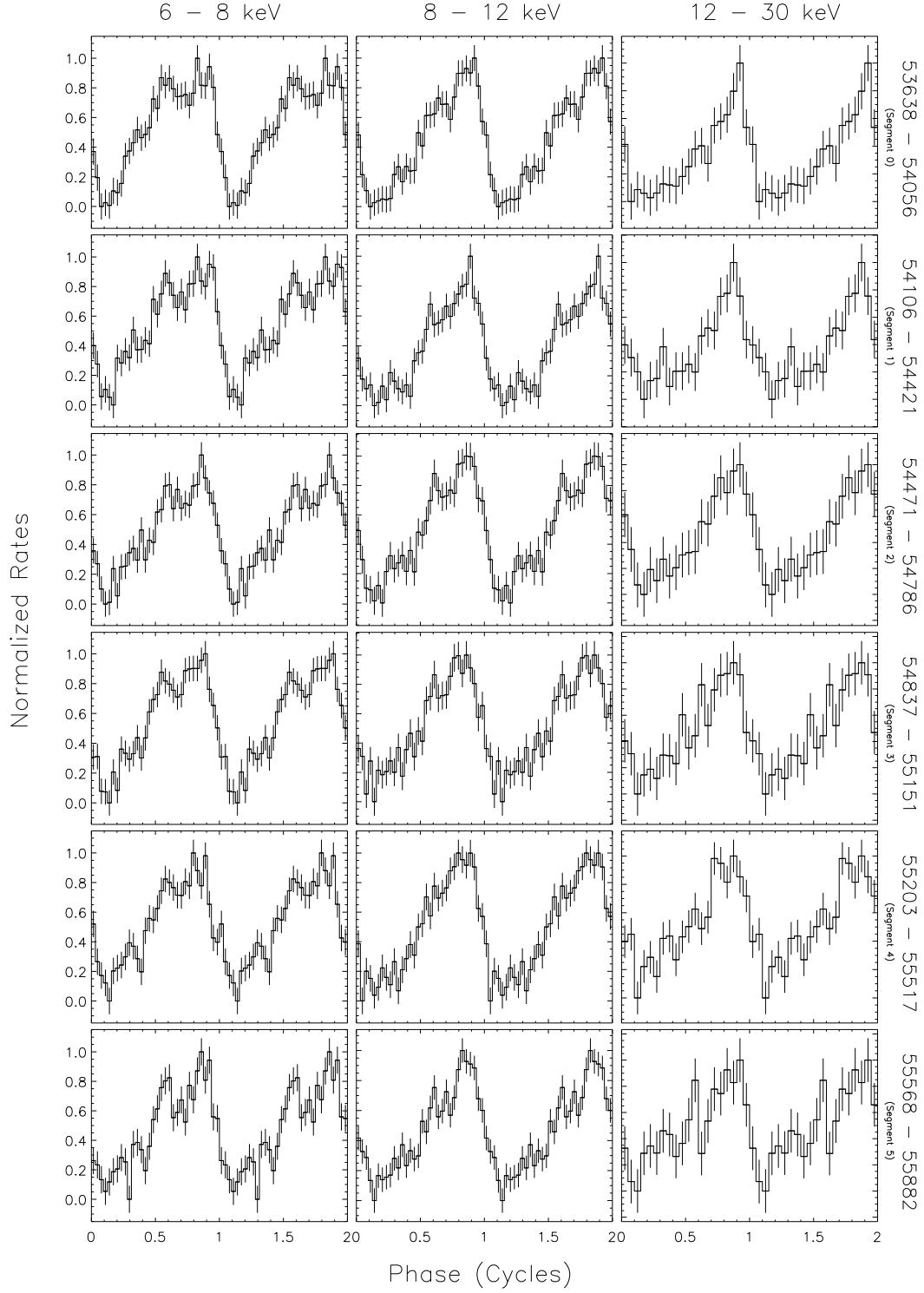


FIG. 4.— Pulse profile history of 1RXS J170849.0-400910 in the energy bands 6–8, 8–12 and 12–30 keV. The labels on the right are the corresponding time intervals of accumulated data. The 12–30 keV profiles are plotted with 20 phase bins due to lower count rate in this energy band.

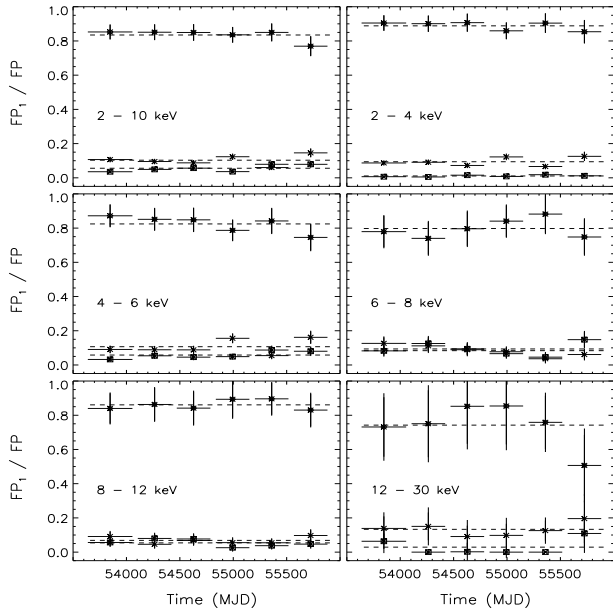


FIG. 5.— Time evolution of the normalized Fourier harmonic powers in the first three harmonics. Dashed lines represent the averaged power of the related harmonic in all segments. The energy intervals in which the powers are calculated are displayed inside the panels.

gap in order to identify it as a possible glitch event. We calculated the total phase error for each gap adopting the timing solutions on both sides of the gaps, and present these results in Table 2.

We then applied the glitch search methodology to  $\sim 250$  day long data segments centered around each gap (gap segment), and evaluated minimum  $\chi^2$  searches as explained above. Best-fit timing solutions are listed in Table 2. Among all gaps, only glitch amplitudes in gap segment 3 (54687–54913) and gap segment 5 (55406–55666) satisfy condition 5. In particular, the glitch amplitude in gap segment 5 is  $\sim 7$  times larger than the noise criterion which makes it a rather strong candidate for a possible glitch event. The putative glitch identified in gap segment 3 has an amplitude  $\sim 4$  times larger than the corresponding minimum noise criterion. The amplitudes of estimated glitch events in gap segments 1, 2 and 4 possess large errors. The rms fluctuations of phase residuals in gap segments are similar in gap segments 1, 2, 3, and 5, while they are much larger in gap segment 4. Note that glitch amplitude in gap segment 4 is affected from an outlier phase measurement (see Figure 8), without which the glitch amplitude becomes even less significant. We, therefore, identified two glitch candidates; a strong case in the gap segment 5, and another one in gap segment 3 which is slightly less robust. We discuss their implications below.

#### 4. DISCUSSION AND CONCLUSIONS

We performed detailed long term timing studies of 1RXS J170849.0-400910 spanning  $\sim 6$  yr. Together with the earlier extensive study of the source by Dib et al. (2008), our investigation considers the entire database of *RXTE* observations of 1RXS J170849.0-400910. In our long-term timing investigations, it was possible to describe the phase shifts with a second order polyno-

mial in only one interval (Segment 4 in Table 1), while all other parts required higher order terms. These results are similar to what has been obtained by Dib et al. (2008), Archibald et al. (2008), and Israel et al. (2007a), confirming the fact that 1RXS J170849.0-400910 is indeed a noisy pulsar.

The pulse profile of 1RXS J170849.0-400910 in the 2–10 keV band does not show any significant variations over the last  $\sim 6$  yr, maintaining its general pulse structure as in the earlier epochs. A minor structure (described as a shoulder above) in the pulse profile below 4 keV becomes stronger with energy and dominates the pulse profiles above 8 keV, as also noted by den Hartog et al. (2008) regarding earlier observations of the source. We also find no significant changes in the rms pulsed count rates (i.e., a measure of the pulsed flux) in the 2–10 keV range. In these respects, 1RXS J170849.0-400910 exhibits an almost stable pulsed X-ray emission behavior. We constructed a coarse energy spectrum of the rms pulsed count rates for each observation segment and found that it becomes gradually harder with time, as indicated by a shallowing power law index.

As a result of  $\sim 14$  yr of *RXTE* observations, three glitches with two different recovery characteristics were unveiled unambiguously, and three candidate glitches were suggested in the time baseline between 1999 and 2005. Such a glitching behavior of 1RXS J170849.0-400910 made this system one of the most frequently glitching pulsars (Israel et al. 2007a; Dall’Osso et al. 2003; Dib et al. 2008). It is important to report the fact that, we do not find any unambiguous glitches in the time interval between 2006 and 2011. However, glitch search in the gaps yielded a strong candidate in gap 5 with glitch amplitude  $\sim 10^{-7}$  which is  $\sim 7$  times larger than the noise in this gap and on the order of largest glitches observed from this source. We identified another candidate in gap segment 3, although it is slightly less robust.

Glitches are generally explained by models involving the neutron star crust, superfluid component of the inner crust or core superfluid and starquakes. The superfluid vortex unpinning model involves the crust and inner crust superfluid (Anderson & Itoh 1975; Alpar et al. 1984a). In this model vortices formed by superfluid are pinned to the neutron-rich nuclei. While the crust spins down due to the electromagnetic torques, a rotational lag between the superfluid component and the crust builds up. When a critical value of rotational lag ( $\delta\Omega \equiv \Omega_s - \Omega_c$ , where  $\Omega_s$  and  $\Omega_c$  are the superfluid’s and crust’s rotational rate, respectively) is reached, vortices suddenly unpin, resulting in transfer of angular momentum to the crust, i.e., glitch. This lag also determines the glitch occurrence time interval. This model is successful in explaining large glitches ( $\Delta\nu/\nu \sim 10^{-6}$ ), such as those observed from the Vela pulsar with an occurrence time interval of  $\sim 2$  yr (Alpar et al. 1981, 1984b).

Another class of models invokes starquakes, which are triggered by the cracking of the solid neutron star when growing internal stresses strain the crust beyond its yield point (Ruderman 1969, 1976, 1991; Baym & Pines 1971). This critical strain can be reached due to several mechanisms: the star spin down causes a progressive decrease of the equilibrium oblateness of the crust (Ruderman 1969, 1991; Franco et al. 2000); variations of the core magnetic field, due to the motion of core superfluid vortices cou-

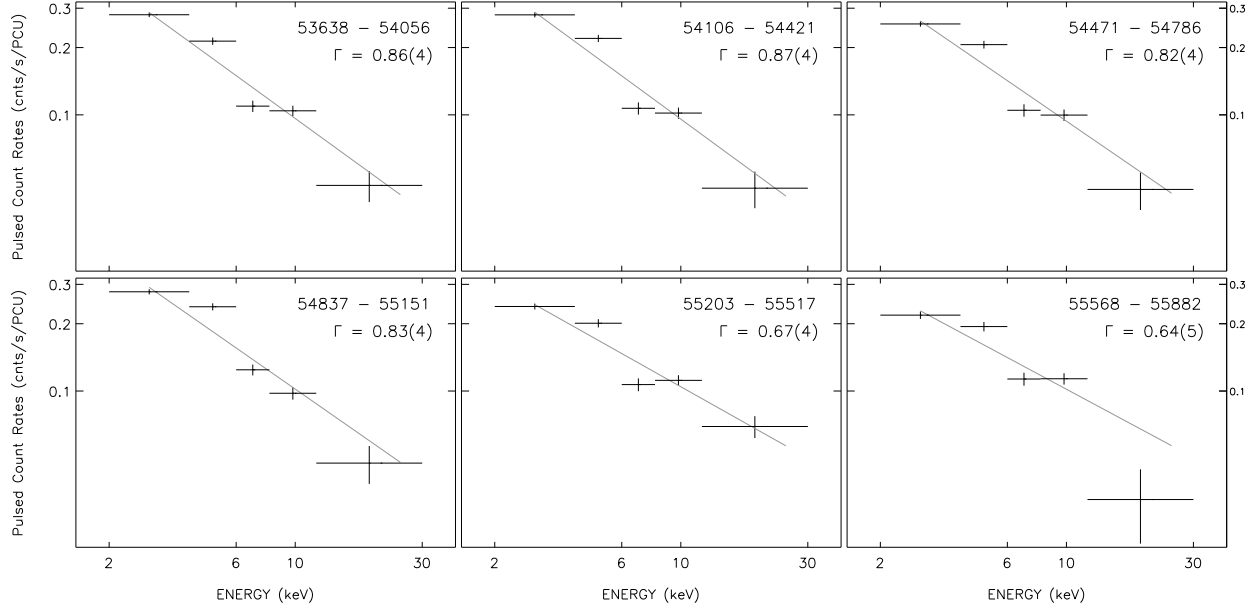


FIG. 6.— Plots of rms pulsed count rates vs. energy. Time intervals within which these plots were obtained are shown in the top-right of each panel. Solid lines show the best fit power law trends to the corresponding energy dependent RMS pulsed count rates. Uncertainties in these power law indices refer to the last digit as shown in parenthesis in each panel.

TABLE 2  
TIMING SOLUTIONS IN THE SEGMENTS INCLUDING THE GAPS

Parameter	Gap Segment 1	Gap Segment 2	Gap Segment 3	Gap Segment 4	Gap Segment 5
Range (MJD)	53952.558–54190.841	54323.309–54575.557	54687.314–54913.097	55048.230–55307.736	55405.757–55665.660
Epoch (MJD)	54106.040	54471.050	54836.804	55202.849	55567.977
Number of TOAs	29	31	27	28	31
$\nu$ (Hz)	0.0908775775(8)	0.090872564(1)	0.090867525(2)	0.090862442(2)	0.090857270(4)
$\dot{\nu}$ ( $10^{-13}$ Hz s $^{-1}$ )	–1.617(2)	–1.584(2)	–1.590(4)	–1.646(3)	–1.638(4)
$t_g$ (MJD)	54174.105	54531.016	54818.531	55245.277	55532.328
$\Delta\nu$ ( $10^{-8}$ Hz)	8(4)	2(2)	6.4(4)	4(1)	12.4(3)
$\Delta\dot{\nu}$ ( $10^{-15}$ Hz s $^{-1}$ )	–43(56)	9(9)	–3(1)	–10(4)	–4.3(8)
rms (phase)	0.0151	0.0165	0.0170	0.0264	0.0156
Gap Range (MJD)	54056–54106	54422–54471	54786–54836	55151–55202	55517–55567
Gap Criterion ( $10^{-8}$ )	2.31	2.15	1.76	0.73	1.74

<sup>a</sup> Values in parenthesis are the uncertainties in the last digits of their associated measurements

pled to it (Srinivasan et al. 1990; Ruderman et al. 1998); and, in strongly magnetized neutron stars, the rapid diffusion of the core magnetic field (or the “turbulent” evolution of the crustal field) provides an alternative channel to produce crustal fractures (Thompson & Duncan 1996; Rheinhardt & Geppert 2002). Dall’Osso et al. (2003), based on the different recovery characteristics of the glitches of 1RXS J170849.0–400910, proposed that they can be explained by a magnetically-driven starquake model since they intrinsically involve local processes and a higher degree of complexity.

In order to discriminate between different possible models, Alpar & Baykal (1994) following Alpar & Ho (1983), investigated the global properties of large pulsar glitches using a sample of 430 pulsars, excluding the Vela pulsar. As these sources are not continuously monitored due to limited telescope times or other observational constraints, there are unavoidable data gaps in between successive pointings. This case puts a serious constraint on the detectability of a glitch if it occurs in a data gap of

a pulsar with noisy timing behavior. They introduced a noise criterion (see Eqn. 5) for significantly detecting frequency jumps in the observational gaps. Therefore, they restricted their analysis to the 19 pulsar glitches with  $\Delta\nu/\nu > 10^{-7}$ . They estimated the physical parameters, e.g., inter-glitch time for the vortex unpinning model and the glitch size for the core-quake model. The parameters of the former model were estimated with two different assumptions for unpinning: First, the critical glitch parameter is taken as  $\delta\Omega$  which is a representative of the number of vortices that is unpinned at the time of the glitch. Second, this parameter is taken as fractional density of the unpinned vortices that is proportional to  $\delta\Omega/\Omega$ , as the density of vortices  $\propto \Omega$ . They also assumed that the probability of observing  $n$  glitches is given by Poisson statistics. Glitch size estimation from the core-quake model is far bigger than the glitch amplitudes of the Vela pulsar and sample mean. Thus, their work statistically excluded the core-quake model. They also compared the parameter estimates of the vortex un-



TABLE 3  
CRITICAL PARAMETER VALUES AND RESULTS OF THE EXPECTANCY ANALYSIS OF  
1RXS J170849.0-400910

Number of glitches (n)	Critical parameter <sup>a</sup> ( $\langle\delta\Omega/\Omega\rangle$ )	Expectancy of Glitches <sup>b</sup>		
		1998–2005	1998–2011	2006–2011
2	$2.3 \times 10^{-4}$	1.8	3.2	1.4
	$2.0 \times 10^{-4}$	2.0	3.6	1.6
	$1.6 \times 10^{-4}$	2.5	4.6	2.0
3	$1.5 \times 10^{-4}$	2.6	4.8	2.1
	$1.4 \times 10^{-4}$	3.0	5.4	2.4
	$1.1 \times 10^{-4}$	3.8	6.9	3.0
6	$7.7 \times 10^{-5}$	5.3	9.2	3.8
	$6.8 \times 10^{-5}$	6.0	10.4	4.2
	$5.4 \times 10^{-5}$	7.6	13.2	5.4

<sup>a</sup> The upper (top), average (middle) and lower values (bottom) for the critical parameter value of the vortex unpinning model.

<sup>b</sup> Calculated using the average value of the  $\dot{\nu}/\nu$  within the specified time range. Timing solutions before 2005 are taken from Dib et al. (2008).

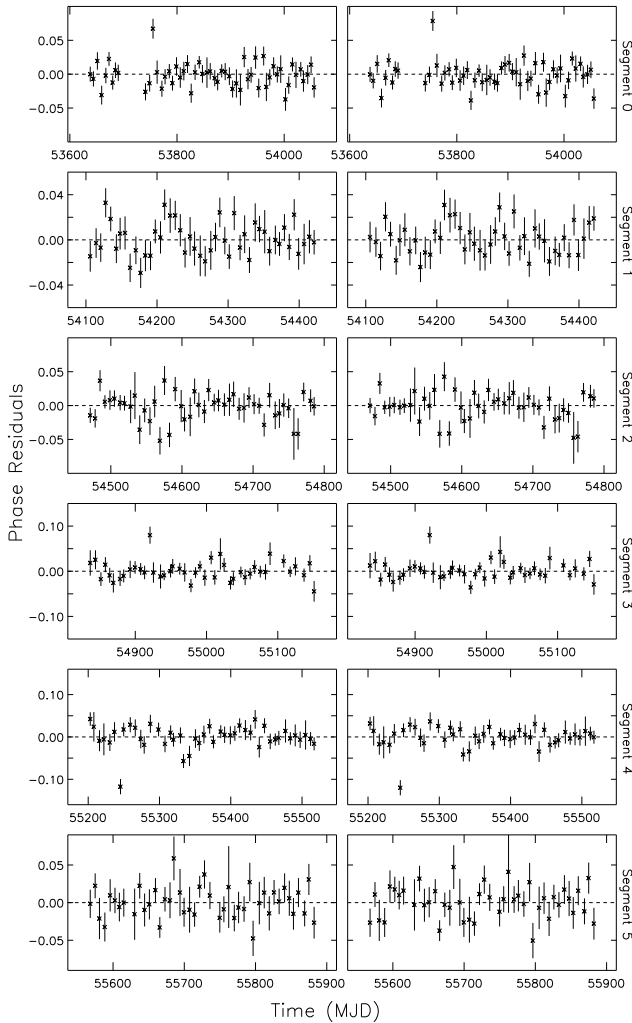


FIG. 7.— (Left column): Phase residuals of the polynomial fit to each data segment. (Right column): Phase residuals of the glitch model fit.

pinning model with those of glitches from Vela and other pulsars, and concluded that the vortex unpinning model with a constant fractional vortex density ( $\langle\delta\Omega/\Omega\rangle$ ) is the most compatible model and can represent an invariant for glitches.

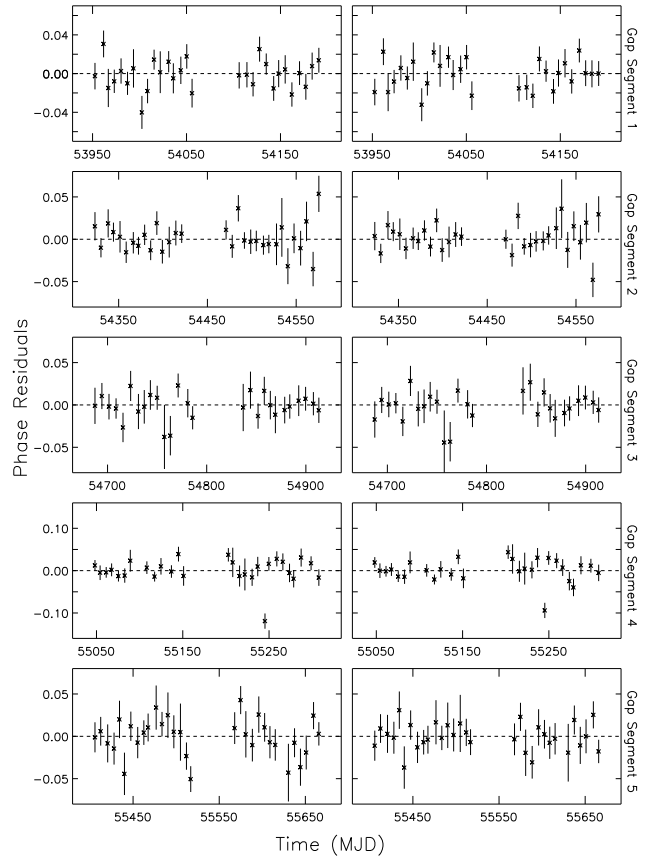


FIG. 8.— (Left column): Phase residuals of the polynomial fit to each gap segment. (Right column): Phase residuals of the glitch model fit.

To test the glitch expectancy within the vortex unpinning model for 1RXS J170849.0-400910 glitches, we applied the same statistical glitch expectancy analysis (see Equation 11 of Alpar & Baykal 1994) and estimated the expected number of glitches using  $\sim 14$  yr of *RXTE* observations. We calculated the critical fractional vortex density of the vortex unpinning model by using the time span between 1998 January and 2005 November, which contains three glitches and three glitch candidates (Dib et al. 2008; Dall’Osso et al. 2003; Israel et al. 2007a). For a single pulsar,  $\dot{\nu}/\nu$  value is not expected

to fluctuate between observations. However, this is not the case for 1RXS J170849.0-400910 as it changes between  $-1.87 \times 10^{-12} \text{ s}^{-1}$  and  $-1.31 \times 10^{-12} \text{ s}^{-1}$  with an average value of  $-1.66 \times 10^{-12} \text{ s}^{-1}$ , which further implies the noisy timing characteristics of the source. Therefore, we performed our calculations for all these three values. First we included the observational gaps into the total time span which, by the chosen noise criterion, restricts our analysis to large glitches with  $\Delta\nu/\nu$  on the order of  $10^{-6}$ . Using  $\dot{\nu}/\nu$  values and observed number of glitches with  $\Delta\nu/\nu \sim 10^{-6}$  (i.e.,  $n = 2$ ), we obtain the upper, lower and average values for critical parameter value of the vortex unpinning model. We note an important fact here that a glitch candidate (i.e., near candidate glitch 2 in Dib et al. (2008)) was reported by Israel et al. (2007a) with a fractional amplitude of  $1.2 \times 10^{-6}$ . If the latter report is correct, the number of large glitches in the 1998–2005 interval would be 3 (i.e.,  $n = 3$ ) which changes the critical parameter. Finally, we excluded all data gaps except the ones with glitches reported in them, and the ones that satisfied the noise criterion in our analysis, and we considered all reported glitches with  $\Delta\nu/\nu \gtrsim 10^{-7}$  (i.e.,  $n = 6$ ) and calculated the critical parameters for this case as well. In Table 3 we list the values of the critical parameter for each of the above-mentioned cases and their corresponding expected number of glitches in the time intervals between 1998–2005, 1998–2011, and 2006–2011. As expected, the average value of the critical parameter yields the observed number of glitches in the 1998–2005 interval. We find that the total number of expected glitches with fractional amplitudes of  $\gtrsim 10^{-6}$  ( $n = 2$  in Table 3) varies between 3.2 and 4.6 if the time baseline spans until the end of the *RXTE* coverage of the source in 2011 November. The number of glitches in the 2006–2011 time range, where we found a strong candidate, were expected to range from 1.4 to 2.0. We then repeated the above procedure, this time excluding all data gaps except the ones with reported candidate glitches. In this case, the noise criterion allows consideration of all glitches with  $\Delta\nu/\nu \sim 10^{-7}$  (i.e.,  $n = 6$ ), and we re-calculated the critical parameters (see Table 3).

Glitch expectancy analysis within the context of vortex unpinning model suggests that 1RXS J170849.0-400910 might have had, on average, two large glitches in 6 yr, corresponding to the interval of 2006–2011 (Table 3). The two significant glitch candidates we identified in gap segments are, therefore, important, since they comprise the observed number to match with the expectancy of the vortex creep model. As far as only glitch statistics is concerned, this case implies that the mechanism leading to the observed glitches in 1RXS J170849.0-400910 is internal. However, where particular glitch characteristics were concerned (e.g., discrepancies in glitch recovery),

the vortex unpinning model is argued to be not sufficient (Dall’Osso et al. 2003).

1RXS J170849.0-400910 is the only member of the magnetar family that has not exhibited energetic X-ray bursts. Almost all other AXPs, that have experienced timing glitches, emitted energetic bursts either in conjunction with (e.g., 1E 2259+586, Woods et al. (2004)) or contemporaneous to their glitches. It is, therefore, suggestive that a common mechanism might be responsible for both glitches and bursts. The dipole magnetic field strength of 1RXS J170849.0-400910 as inferred from its spin period and spin-down rate is about  $4.6 \times 10^{14} \text{ G}$ , that is strong enough to produce significant deformation in the neutron star crust and eventually lead to the release of energy via bursts (Thompson & Duncan 1995). Nevertheless, the condition on 1RXS J170849.0-400910 has not given rise to any observable bursts, even though it has experienced the largest number of glitches among all magnetars. While a common mechanism could reproduce coincident energetic bursts and glitches in general, it might be generating glitches but not detectable enhancements and bursts in 1RXS J170849.0-400910, possibly due to this source having slightly lower crust shear modulus, so that the release of less energy can still produce breaks in the crust. The energetic bursts, however, are not accounted for within the context of the vortex unpinning model which appears to be favored for this source in our statistical investigations.

Recently Eichler & Shaisultanov (2010) suggested that vortices can be unpinned mechanically via oscillations rather than by a sudden heat release. According to their estimation, the relative velocity between the crust and superfluid, which is generated by the mechanical energy release at the depths below 100 m, can exceed the critical velocity lag and unpin the vortices. In order to explain the radiatively silent glitches seen in some AXPs (as in the case of 1RXS J170849.0-400910) they proposed that mechanically triggered glitch event might not be accompanied by a long-term X-ray brightening since a glitch can be triggered by a less energy release. In this picture, the origin of X-ray brightening is also through mechanical energy release and these flux enhancements are expected to be accompanied with glitch events. This scenario can be diagnosed through the exact timing of glitches with radiative enhancements (Eichler & Shaisultanov 2010).

We would like to thank M. Ali Alpar and the anonymous referee for helpful comments. SŞM acknowledges support through the national graduate fellowship program of the Scientific and Technological Research Council of Turkey (TÜBİTAK).

## REFERENCES

- Alpar, M. A., Anderson, P.W., Pines, D., & Shaham, J. 1981, *ApJ*, 249, L29  
 Alpar, M. A. & Ho, C. 1983, *MNRAS*, 204, 655  
 Alpar, M. A., Anderson, P.W., Pines, D., & Shaham, J. 1984a, *ApJ*, 276, 325  
 Alpar, M. A., Anderson, P. W., Pines, D., & Shaham, J. 1984b, *ApJ*, 278, 791  
 Alpar, M. A., & Baykal, A. 1994, *MNRAS*, 269, 849  
 Anderson, P. W., & Itoh, N. 1975, *Nature*, 256, 25  
 Archibald, A. M., Dib, R., Livingstone, M. A., & Kaspi, V. M. 2008, in *AIP Conf. Ser.* 983, 40 Years of Pulsars: Millisecond Pulsars, Magnetars and More, eds. C. Bassa, Z. Bassa, A. Cumming & V. M. Kaspi (Melville, NY: AIP), 265  
 Baym, G., & Pines, D. 1971, *Ann.Phys.*, 66, 816  
 Campana, S., Rea, N., Israel, G. L., Turolla, R., & Zane, S. 2007, *A&A*, 463, 1047  
 Dall’Osso, S., Israel, G. L., Stella, L., Possenti, A., & Perozzi, E. 2003, *ApJ*, 599, 485  
 Dall’Osso, S., Granot, J., & Piran, T. 2012, *MNRAS*, 422, 2878

- den Hartog, P. R., Kuiper, L., & Hermsen, W. 2008, *A&A*, 489, 263
- Dib, R., Kaspi, V. M., & Gavriil, F. P. 2008, *ApJ*, 673, 1044
- Dib, R., Kaspi, V. M., & Gavriil, F. P. 2009, *ApJ*, 702, 614
- Eichler, D., & Shaisultanov, R. 2010, *ApJ*, 715, 142
- Franco, L. M., Link, B., & Epstein, R. I. 2000, *ApJ*, 543, 987
- Gavriil, F. P., Kaspi, V. M., & Woods, P. M. 2002, *Nature*, 419, 142
- Gavriil, F. P., Dib, R., & Kaspi, V. M. 2011, *ApJ*, 736, 138
- Götz, D. et al. 2007, *A&A*, 475, 317
- Groth, E. J., 1975, *ApJS*, 286, 29, 285
- İçdem, B., Baykal, A., & İnam, S. Ç. 2012, *MNRAS*, 419, 3109
- Israel, G. L., Covino, L., Stella, L., Campana, S., Haberl, F., & Mereghetti, S. 1999, *ApJ*, 514, L107
- Israel, G. L., Götz, D., Zane, S., Dall’Osso, S., Rea, N., & Stella, L., 2007a, *A&A*, 476, L9
- Israel, G. L., Campana, S., Dall’Osso, S., Munro, M. P., Cummings, J., Perna, R., & Stella, L. 2007b, *ApJ*, 664, 448
- Kaspi, V. M., Chakrabarty, D., & Steinberger, J. 1999, *ApJ*, 525, L33
- Kaspi, V. M., Lackey, J. R., & Chakrabarty, D. 2000, *ApJ*, 537, L31
- Kaspi, V. M., & Gavriil, F. P. 2003, *ApJ*, 596, L71
- Kaspi, V. M., Gavriil, F. P., Woods, P. M., et al. 2003, *ApJ*, 588, L93
- Kumar, H. S., & Safi-Harb, S. 2010, *ApJ*, 725, L191
- Lin, L., et al. 2011, *ApJ*, 740, L16
- Markwardt, C.B. 2009, in *Astronomical Society of the Pacific Conference Series*, Vol. 411, *Astronomical Data Analysis Software and Systems XVIII*, ed. D.A. Bohlender, D. Durand & P. Dowler, 251
- Morii, M., Kawai, N., & Shibasaki, N. 2005, *ApJ*, 622, 544
- Pines, D., Shaham, J., Alpar, M. A., & Anderson, P.W. 1980, *Prog.Theor.Phys.Suppl.*, 69, 376
- Pons, J. A., & Rea, N. 2012, *ApJ*, 750, L6
- Radhakrishnan, V., & Manchester, R. N. 1969, *Nature*, 222, 228
- Rea, N., et al. 2005, *MNRAS*, 361, 710
- Rea, N., et al. 2007, *Ap&SS*, 308, 505
- Rea, N., & Esposito, P. 2011, in *High Energy Emission from Pulsars and their Systems*, ed. D. F. Torres & N. Rea, (Berlin: Springer), 247
- Rheinhardt, M., & Geppert, U. 2002, *Phys. Rev. Lett.*, 88, 101103
- Richards, D. W., & Comella, J. M. 1969, *Nature*, 222, 551
- Ruderman, M. 1969, *Nature*, 223, 597
- Ruderman, M. 1976, *ApJ*, 203, 213
- Ruderman, M. 1991, *ApJ*, 382, 587
- Ruderman, M., Zhu, T., & Chen, K. 1998, *ApJ*, 492, 267
- Srinivasan, G., Bhattacharya D., Muslimov A. G., & Tsygan A.J. 1990, *Current Science*, 59, 31
- Sugizaki, M., Nagase, F., Torii, K., Kinugasa, K., Asanuma, T., Matsuzaki, K., Koyama, K., & Yamauchi, S. 1997, *PASJ*, 49, L25
- Thompson, C., & Duncan, R. C. 1995, *MNRAS*, 275, 255
- Thompson, C., & Duncan, R. C. 1996, *ApJ*, 473, 322
- Thompson, C., Lyutikov, M., & Kulkarni, S. R. 2002, *ApJ*, 574, 332
- van der Klis, M. 1989, in *Timing Neutron Stars*, eds. H. Ögelman & E. P. J. van den Heuvel (Dordrecht: Kluwer), 27
- Vaughan, B. A., et al. 1994, *ApJ*, 435, 362
- Weltevrede, P., Johnston, S., & Espinoza, C. M. 2011, *MNRAS*, 411, 1917
- Woods, P.M., et al. 2004, *ApJ*, 605, 378
- Woods, P.M., Kaspi, V.M., Gavriil, F. P., & Airhart, C. 2011, *ApJ*, 726, 37
- Zhu, W., & Kaspi, V. M. 2010, *ApJ*, 719, 351